Zoltan Dombovari[1]
e-mail: dombo@mm.bme.hu

Gabor Stepan
e-mail: stepan@mm.bme.hu

Department of Applied Mechanics,
Budapest University of Technology
and Economics,
Budapest H-1521, Hungary

The Effect of Helix Angle Variation on Milling Stability

Helical milling tools of nonuniform helix angles are widely used in manufacturing industry. While the milling tools with these special cutting edges are already available in the market, their cutting dynamics has not been fully explored. Also, there have been several attempts to introduce complex harmonically varied helix tools, but the manufacturing of harmonic edges is extremely difficult, and their effect on cutting dynamics is not clear either. In this study, a general mechanical model is introduced to predict the linear stability of these special cutters with optional continuous variation of the helix angle. It is shown that these milling tools cause distribution in regeneration. The corresponding time-periodic distributed delay differential equations are investigated by semi-discretization. This work points out how the nonuniform and harmonically varied helix cutters behave in case of high and low cutting speed applications. [DOI: 10.1115/1.4007466]

1 Introduction

Some machining processes like boring, turning, and milling are subjected to regenerative effect [1,2] due to the repeating surface pattern that continuously stores the relative vibration between the tool and the workpiece. Because of the rotation, the "stored" past state excites the system after a certain time during the cutting operation. This effect can cause the instability of the stationary cutting operation.

Mathematically, the regeneration can be described by a delay differential equation (DDE) [3], which has time-periodic coefficients [4] in case of milling operations. These equations generate infinite dimensional phase spaces similarly to the partial differential equations [5], which require special (numerical) techniques to investigate [6]. Moreover, in the case of variable helix tools, the time-periodic DDE has distributed regeneration, that is, instead of one specific discrete delay, an interval of delays operates with strengths defined by a weight distribution function. This is a unique direct mechanical example for dynamical systems that can be described by distributed DDEs besides the short delay effect for process damping [7] and some shimmy vibration models [8].

These special type of cutters are effective in the same way as other techniques known in the machine tool industry used to avoid chatter: they are all based on the "variation" or "perturbation" of the regeneration. The spindle speed variation [9,10] causes time dependent delay, the serrated cutter [11,12] causes piecewise smooth switching between discrete delays, while the variable pitch tools operate with several discrete delays [13,14] instead of the single delay of conventional milling.

In this study, we show that the tools with helix variation can be described by distributed DDEs. This way, we extend the mathematical modeling of milling processes initiated in the previous works by Refs. [15–20].

In the first section, we construct the geometric model of milling tools with generally varied helices. In the mechanical model, linear cutting force characteristics is considered acting along the cutting edges. We devote a section for the weight functions of the distributed time delays, and we give two examples how they look like in case of nonuniform and harmonically varied helices. In the last section, we present stability calculations by means of the semi-discretization (SD) method [21].

2 Mechanics of Variable Helix Cutter

In this section, after the geometric interpretation of a general helix variation, the connection between the local cutting force distribution and the distributed delays is introduced.

2.1 General Variable Helix Geometry. The so-called lag angle $\varphi_{\eta,i}(z)$ is the angle with which the local edge portion at level z is behind relative to the beginning of the edge at zero level. In case of constant helix $\bar{\eta}_i$, this is a linear distribution $\varphi_{\bar{\eta},i}(z) = (z/R)\tan\bar{\eta}_i$ along the z axis [22] if the radius R is constant. For the sake of generality, we consider a general variation $\delta_i(z)$ around a mean helix angle $\bar{\eta}_i$ of the ith edge as (cf. Fig. 1)

$$\varphi_{\eta,i}(z) = \varphi_{\bar{\eta},i}(z) - \delta_i(z), \quad i = 1, 2, \ldots, N \tag{1}$$

where N denotes the number of flutes. The local helix angle can be expressed from the continuously changing lag angle as

$$\tan\eta_i(z) = R\varphi'_{\eta,i}(z) \tag{2}$$

Substituting the z derivative of Eq. (1) into Eq. (2), we obtain the following expression for the local helix angle at the ith edge:

$$\eta_i(z) = \arctan(\tan\bar{\eta}_i - R\delta'_i(z))$$

This continuous variation of the helix causes the variation on the pitch angle, too (cf. Fig. 1), that is

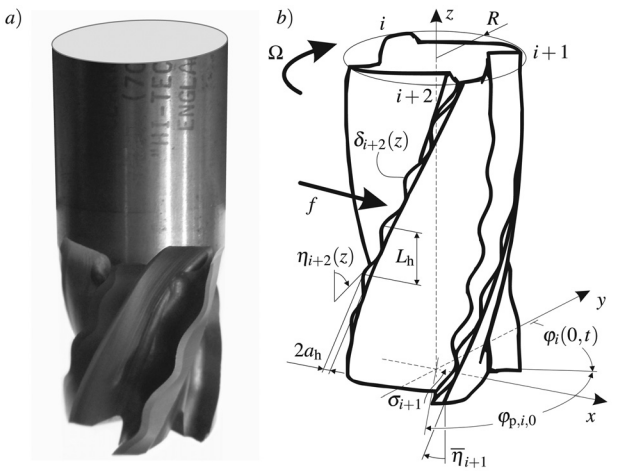

Fig. 1 A real implementation (*a*) and the sketch (*b*) of the milling cutter with harmonically varied helix. (The real tool was provided by Prof. Gy. Matyasi: see Acknowledgment.)

[1]Corresponding author.

Contributed by the Manufacturing Engineering Division of ASME for publication in the JOURNAL OF MANUFACTURING SCIENCE AND ENGINEERING. Manuscript received February 24, 2012; final manuscript received August 9, 2012; published online September 25, 2012. Assoc. Editor: Tony Schmitz.

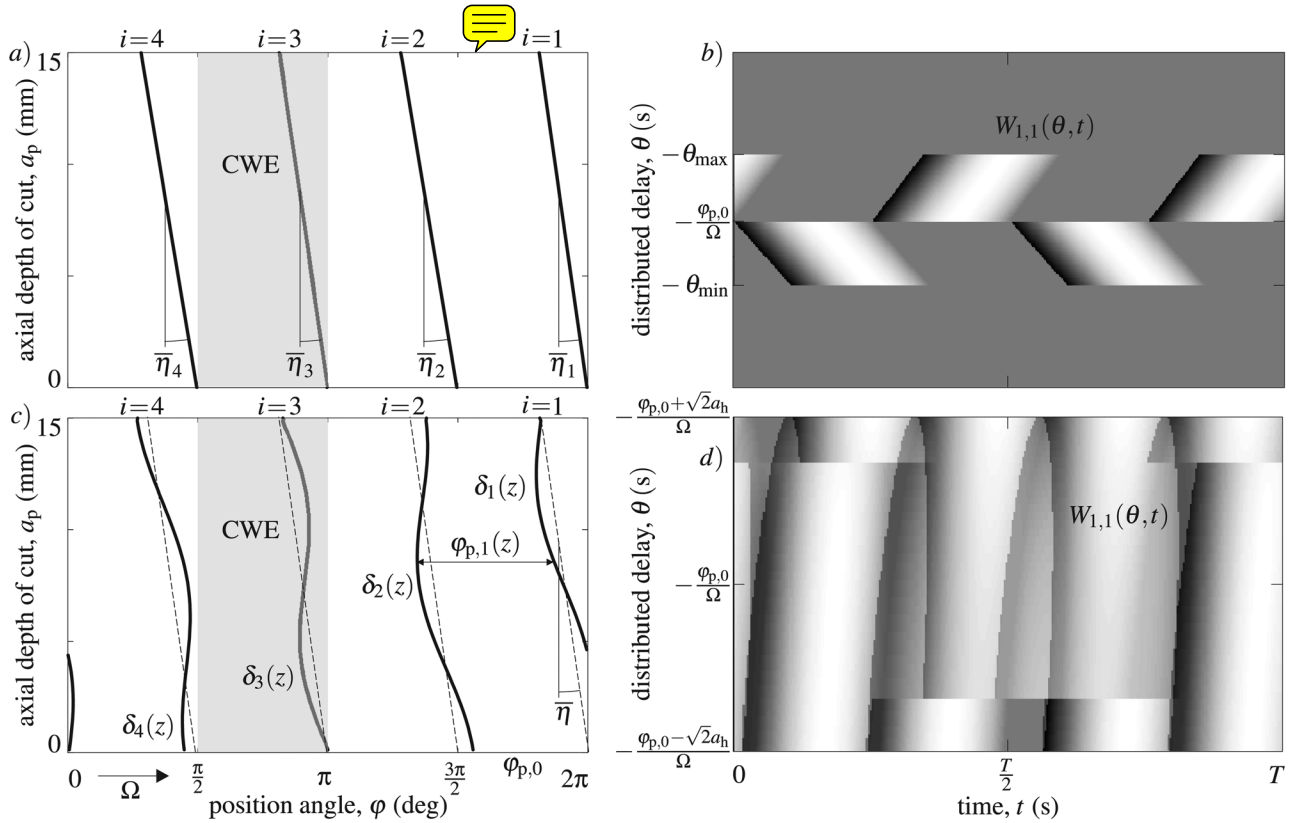

Fig. 2 Edge pattern of nonuniform and harmonically varied helix tools (left panels) and the corresponding weight distributions (right panels). Minimum, zero level, and maximum values are denoted by black, middle gray (see top part of panel (*b*)), and white in panels (*b*) and (*d*).

$$\varphi_{p,i}(z) = \varphi_{p,i,0} + \varphi_{\eta,i}(z) - \varphi_{\eta,i+1}(z)$$

where $\varphi_{p,i,0} = \varphi_{p,i}(0)$ is the ith initial pitch angle considered at level $z = 0$. Note that, in case of a cutter that has only nonuniform constant helix angles $\bar{\eta}_i$ without any variation around ($\delta_i = 0$), the variation of the pitch angle is linear

$$\varphi_{p,i}(z) = \varphi_{p,i,0} + \frac{\tan\bar{\eta}_i - \tan\bar{\eta}_{i+1}}{R} z \tag{3}$$

while in case of a cutter that has uniform mean helix angles $\bar{\eta}_i = \bar{\eta}$ with variations $\delta_i(z)$, the pitch angles are

$$\varphi_{p,i}(z) = \varphi_{p,i,0} + \delta_i(z) - \delta_{i+1}(z) \tag{4}$$

Remark that milling tools corresponding to Eq. (3) are already available in the market.

In both cases, the continuous variation of the pitch angles causes continuous variation in the regenerative effect, since the regenerative delays between subsequent edges at level z has the following direct connection with the local pitch angles:

$$\tau_i(z) = \frac{1}{\Omega}\varphi_{p,i}(z) \tag{5}$$

where Ω is the angular velocity of the tool. Accordingly, milling processes that use variable helix tools are subjected to infinitely many delays as opposed to delay(s) occurring in milling processes with conventional, uniform helix tools [11,23].

2.2 Derivation of Regenerative Milling Force. The standard approximation is used here when the originally trochoid paths of the local edges are approximated by circles, that is

$$h_i(z,t) \approx g_i(z,t)\mathbf{r}_i(z,t)\mathbf{n}_i(z,t)$$

where the local movement of subsequent edge portions and the local normal vectors of the edges can be expressed as

$$\mathbf{r}_i(z,t) = \Delta\mathbf{r}_i(z,t) + \begin{bmatrix} f\frac{\varphi_{p,i}(z)}{2\pi} \\ 0 \\ 0 \end{bmatrix}, \quad \mathbf{n}_i(z,t) = \begin{bmatrix} \sin\varphi_i(z,t) \\ \cos\varphi_i(z,t) \\ 0 \end{bmatrix} \tag{6}$$

respectively, and f is the feed per revolution. The so-called screen function $g_i(z,t)$ takes the radial immersion into account. Its actual form is

$$g_i(z,t) = \begin{cases} 1, & \text{if } \varphi_{en} < (\varphi_i(z,t) \bmod 2\pi) < \varphi_{ex}, \\ 0, & \text{otherwise,} \end{cases}$$

where the entry angle φ_{en} and the exit angle φ_{ex} are measured clockwise from the (y) axis (see Fig. 1). This basically describes box-like cutter-workpiece engagement (CWE) [24] (see gray regions in Figs. 2(*a*) and 2(*c*)). The term that contains the regeneration in Eq. (6) is

$$\Delta\mathbf{r}_i(z,t) = \mathbf{r}(t) - \mathbf{r}(t - \tau_i(z))$$

The position angle of the ith local edge is given by (cf. Fig. 1)

$$\varphi_i(z,t) = \Omega t + \sum_{k=1}^{i-1} \varphi_{p,i}(z) - \varphi_{\eta,1}(z)$$

Having the angular position of the tool edge, the local specific force can be determined in the local t (tangential), r (radial), and a (axial) coordinate system (*tra*), that is

$$\mathbf{f}_{tra,i}(z,t) = -\mathbf{f}(h_i(z,t))$$

where $\mathbf{f}(h)$ is the empirical cutting force characteristics. It is important to notice that the applied force model has to follow the continuously changing helix angle (e.g., orthogonal to oblique transformation [22]). The specific force can be rewritten in Cartesian system using the following transformation:

$$\mathbf{f}_i(z,t,\mathbf{r}_t(\theta)) = g_i(z,t)\mathbf{T}_i(z,t)\mathbf{f}_{tra,i}(z,t)$$

where the negative signs are related to the relative positions of the coordinate systems involved and the transformation matrix between the (*tra*) and (*xyz*) coordinate systems has the form

$$\mathbf{T}_i(z,t) = \begin{bmatrix} \cos\varphi_i & \sin\varphi_i & 0 \\ -\sin\varphi_i & \cos\varphi_i & 0 \\ 0 & 0 & 1 \end{bmatrix}$$

with $\varphi_i := \varphi_i(z,t)$. The sum of all specific force components along the edges and for all flutes gives the resultant cutting force

$$\mathbf{F}(t,\mathbf{r}_t(\theta)) = \sum_i^N \int_{\sigma_i} \mathbf{f}_i(z(\sigma_i),t,\mathbf{r}_t(\theta))\mathrm{d}\sigma_i, \quad \mathrm{d}\sigma_i = \frac{\mathrm{d}z}{\cos\eta_i(z)}$$

where σ_i is the arc length coordinate of the ith flute (see Fig. 1). The $\mathbf{r}_t(\theta) = \mathbf{r}(t+\theta)$ is the shift function [3,5], which represents the actual and the past states of the delayed system, since $\theta \in [-\tau_{\max}, 0](\tau_{\max} = \max_{i,z} \tau_i(z))$.

2.3 Milling Dynamics. The milling process is considered in modal space where the governing equation has the following matrix form:

$$\ddot{\mathbf{q}}(t) + [2\xi_k\omega_{\mathrm{n},k}]\dot{\mathbf{q}}(t) + [\omega_{\mathrm{n},k}^2]\mathbf{q}(t) = \mathbf{U}^{\mathrm{T}}\mathbf{F}(t,\mathbf{U}\,\mathbf{q}_t(\theta)) \tag{7}$$

where $[2\xi_k\omega_{\mathrm{n},k}]$ and $[\omega_{\mathrm{n},k}^2]$ are diagonal matrices that contain the modal damping ratios and the natural angular frequencies of the modes ($k = 1,2,\ldots,N_q$), while $\mathbf{U}$ is the mass-normalized modal transformation matrix (as constructed in Ref. [11]), which connects the spatial and the modal space as $\mathbf{r}_t(\theta) = \mathbf{U}\mathbf{q}_t(\theta)$.

If we consider the perturbation $\mathbf{q}(t) = \mathbf{q}_{\mathrm{p}}(t) + \mathbf{u}(t)$ around the periodic stationary solution $\mathbf{q}_{\mathrm{p}}(t+\theta) = \mathbf{q}_{\mathrm{p}}(t+T+\theta) =: \mathbf{q}_{\mathrm{p},t}(\theta)$, the linearization of Eq. (7) leads to a time-periodic system [4]

$$\ddot{\mathbf{u}}(t) + [2\xi_k\omega_{\mathrm{n},k}]\dot{\mathbf{u}}(t) + [\omega_{\mathrm{n},k}^2]\mathbf{u}(t) = \mathbf{U}^{\mathrm{T}}\sum_{i=1}^N \int_z \mathbf{C}_i(z,t)(\mathbf{u}_t(-\tau_i(z)) - \mathbf{u}_t(0))\mathrm{d}z$$

This can be rewritten in a time-periodic distributed delay form as

$$\ddot{\mathbf{u}}(t) + [2\xi_k\omega_{\mathrm{n},k}]\dot{\mathbf{u}}(t) + ([\omega_{\mathrm{n},k}^2] + \mathbf{C}(t))\mathbf{u}(t) = \int_{-\tau_{\max}}^{-0} \mathbf{W}(\theta,t)\mathbf{u}_t(\theta)\mathrm{d}\theta \tag{8}$$

The weight distribution can be expressed in the following form:

$$\mathbf{W}(\theta,t) = \sum_{i=1}^N \sum_{l=1}^{N_{\mathrm{inv},i}} \mathbf{U}^{\mathrm{T}} \frac{\mathrm{D}_{\mathbf{q}_t(\theta)}\mathbf{f}_i\left(z_{i,l}(\theta),t,\mathbf{U}\mathbf{q}_{\mathrm{p},t}(\theta)\right)}{\cos\eta_i(z_{i,l}(\theta))}|z'_{i,l}(\theta)| \tag{9}$$

in the delayed-time interval $\theta \in [-\tau_{\max}, 0)$. In Eq. (9), D denotes gradient now w.r.t. $\mathbf{q}_t(\theta)$ and $z_{i,l}(\theta)(l = 1,2,\ldots,N_{\mathrm{inv},i})$ are the lth local inverse functions of $\theta = -\tau_i(z)$. The term $|z'_{i,l}(\theta)|$ in Eq. (9) represents the integration by substitution with $\mathrm{d}z = |z'_{i,l}(\theta)|\mathrm{d}\theta$. The coefficient matrix of the present solution in Eq. (8) is originated from the weight function as

$$\mathbf{C}(t) := \mathbf{U}^{\mathrm{T}}\mathrm{D}_{\mathbf{q}_t(0)}\mathbf{F}(t,\mathbf{U}\mathbf{q}_{\mathrm{p},t}(\theta)) = \int_{-\tau_{\max}}^{-0} \mathbf{W}(\theta,t)\mathrm{d}\theta \tag{10}$$

3 Weights of Distributed Delays

As it was shown at Eq. (8), continuously changing helices cause continuous variation in the delays. This means that the axial force distribution can be considered as a weight distribution Eq. (9) with respect to the delayed time θ. Because of the time periodicity of the original system, the weight distribution is time periodic too, that is, $\mathbf{W}(\theta,t) = \mathbf{W}(\theta,t+T)$, where T is the principal period of the milling process. According to Eq. (10), the following is also true: $\mathbf{C}(t) = \mathbf{C}(t+T)$.

In Fig. 2, one can follow how the weight distribution $\mathbf{W}(\theta,t)$ is originated in the edge pattern and the CWE (shaded areas). It can be realized that the variation of helices (the axial variation on pitch angles) "smear" the "sharp" effect of a constant delay occurring in case of conventional milling tool (see Figs. 2(*b*) and 2(*d*)), where the $-\varphi_{\mathrm{p},0}/\Omega$ denotes the corresponding discrete delay value that would be described by a Dirac delta function as a weight distribution. Note that all the examples shown in Fig. 2 are constructed at $\Omega = n = 5000$ rpm and $a_{\mathrm{p}} = 15$ mm in case of half immersion down-milling. The tool used for the simulation has diameter $D = 2R = 30$ mm and the number of flutes is $N = 4$.

A typical pattern caused by nonuniform helices can be seen at Fig. 2(*b*) (the gray-scale refers to weights with white for high values and black for low values). Apart of the fact that an interval of distributed delays appears instead of a discrete delay, it is also true that subsequent flutes with varying helices induce wide delay intervals compared to the discrete delay of conventional milling. The realized repeatable pattern assumes $\bar{\eta}_i = 30, 34, 30, 34$ deg in Fig. 2(*a*). One may find more complex patterns, too, but it will remains linearly distributed in case of nonuniform constant helices as shown in Fig. 2(*b*).

The other case in Fig. 2(*d*) shows the weight distribution for harmonically varied helix tool with $L_{\mathrm{h}} = 15$ mm wavelength and $a_{\mathrm{h}} = 10$ deg variation amplitude. Here, the variations $\delta_i(z)$ from Eq. (1) have the following form:

$$\delta_i(z) = a_{\mathrm{h}} \sin\left(2\pi\frac{z}{L_{\mathrm{h}}} + \psi_{\mathrm{h},i}\right) \tag{11}$$

where $\psi_{\mathrm{h},i}$ are the phase shifts between harmonic variations of subsequent flutes (see Fig. 2(*c*)). In case of uniform phase shifts, we have $\psi_{\mathrm{h},i} = \sum_{k=1}^{i-1} \varphi_{\mathrm{p},i,0}$. According to Eqs. (4) and (11), the varying pitch angles related to the ith flute can be expressed as

$$\varphi_{\mathrm{p},i}(z) = \varphi_{\mathrm{p},i,0} + \Phi_{\mathrm{p},i} \sin\left(2\pi\frac{z}{L_{\mathrm{h}}} + \varepsilon_i\right)$$

where $\Phi_{\mathrm{p},i}$ and ε_i are the amplitudes and the phase shifts of the variations. Note that $\Phi_{\mathrm{p},i} = \sqrt{2}a_{\mathrm{h}}$ and $\varepsilon_i = \frac{\pi}{4}, \frac{3\pi}{4}, \frac{5\pi}{4}, \frac{7\pi}{4}$ in case of a $N = 4$ fluted tool with uniform initial pitch angles $\varphi_{\mathrm{p},0} := \varphi_{\mathrm{p},i,0} = \frac{\pi}{2}$. This obviously means that the larger the variation amplitude a_{h} is, the wider the weight distribution will be. One may expect a continuous weight function for the delay distribution due to the presence of harmonically varied helix and the continuous change of variables, but this is not the case in Fig. 2(*d*). There are three sources of possible nonsmoothness in the weight function of delay distribution. On one hand, the chip thickness may still change abruptly, too and so does the cutting force. This means possible sharp change in the chip thickness shifted in time t as depicted in Fig. 2(*d*). On the other hand, there can be nonsmoothness along the distributed time delay θ, too, since neighboring delay intervals can be related to different chip thickness values in the CWE as it is observable in Fig. 2(*c*) as one follow how and where the $(i+4)$th edge enters into the CWE. Moreover, the occurrence of different delays can change instantly too, especially, when a cutting edge enters or leaves the

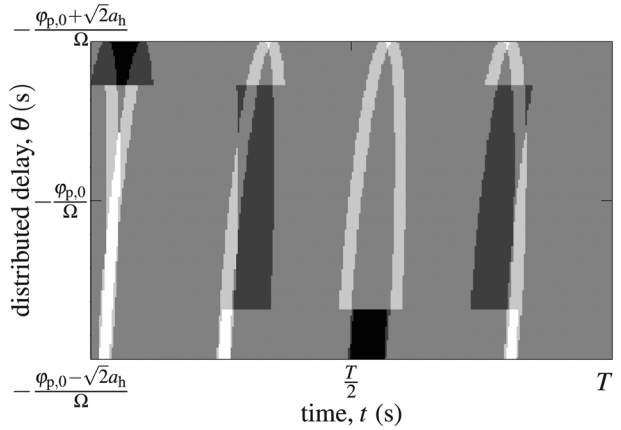

Fig. 3 Occurrence density of delays (black is zero, while white is four occurrences)

workpiece. This effect is presented in the delay occurrence density plot depicted in Fig. 3 in case of harmonic variation of helices ($L_h = 15$ mm and $a_h = 10$ deg). Note that there are delay intervals, which are not acting in some parts of the period at all (black means zero occurrence, while white indicates four occurrences in Fig. 3).

4 Linear Stability

The linear stability of dynamical systems like Eq. (8) can be investigated by the SD method [21,25]. Note that the cutting tools dealt with in this paper need discretization along the axial direction to cover correctly the waves along the edges. However, the discretization along the distributed delay θ should result in a proper representation of the weight distributions $\mathbf{W}(\theta, t)$, which is not an obvious task due to the above described discontinuity properties of the distributions.

In short, the semi-discretization combined by the Floquet theorem [4] can approximate the so-called monodromy operator of time-periodic distributed DDEs that maps the current state $\mathbf{u}_t(\theta)$ of the system to the state $\mathbf{u}_{t+T}(\theta)$ after a period. The discrete counterpart of the monodromy operator is the transition matrix, which connects the current discretized state $\mathbf{z}_i$ with the state $\mathbf{z}_{i+k}$ after a period, that is

$$\mathbf{z}_{i+k} = \Phi \mathbf{z}_i \tag{12}$$

where $\mathbf{z}_i = \mathrm{col}(\mathbf{u}_{t_i}(0), \dot{\mathbf{u}}_{t_i}(0), \mathbf{u}_{t_i}(-\Delta\theta), \mathbf{u}_{t_i}(-2\Delta\theta), \ldots, \mathbf{u}_{t_i}(-r\Delta\theta))$. The delay resolution and the delay time step are $r = \mathrm{int}(\tau_{\max}/\Delta\theta + 1/2)$ and $\Delta\theta = \Delta t = T/k$, respectively. Note that k is the resolution in the time period T and r is the resolution in the maximum delay $\tau_{\max}$. The transition matrix Φ can be determined using the linear maps $\mathbf{B}_i$ in subsequent time intervals $t \in [t_i, t_i + \Delta t]$

$$\Phi = \mathbf{B}_{i+k-1}\mathbf{B}_{i+k-2}\ldots\mathbf{B}_{i+1}\mathbf{B}_i \tag{13}$$

The linear map $\mathbf{B}_i$ is basically the semi-discretized version of the solution operator of Eq. (8) at Δt if $\mathbf{u}_{t_i}(\theta)$ were the initial state. The $\mathbf{B}_i$ contains the exact analytical solutions of finite number of linear ODEs defined over the discretized state $\mathbf{z}_i$ in the time interval $t \in [t_i, t_i + \Delta t]$ [21].

It is important to mention that, due to the necessary fine mesh on the axial direction, the multiplications defined at Eq. (13) can be time consuming. Therefore, special techniques can be used [26,27] in order to decrease the computational cost of the problem.

5 Numerical Results by Semi-discretization

The linear stability properties of some milling operations performed with variable helix tool are shown in Figs. 4 and 5 in comparison with the linear stability of a conventional $N = 4$ fluted helix tool with $\bar{\eta} = 30$ deg helix angle (see dashed lines in all panels of Figs. 4 and 5). The process is symmetric interrupted milling characterized by the immersion angle $\Delta\varphi = \varphi_{ex} - \varphi_{en}$, that is $\varphi_{en} = \pi/2 - \Delta\varphi/2$ and $\varphi_{ex} = \pi/2 + \Delta\varphi/2$. Two identical dominant modes are considered in the parallel and perpendicular directions to the feed. The modal parameters can be found in Table 1 and the tangential and radial cutting coefficients were $K_{c,t} = 900$ MPa and $K_{c,r} = 300$ MPa, respectively. These

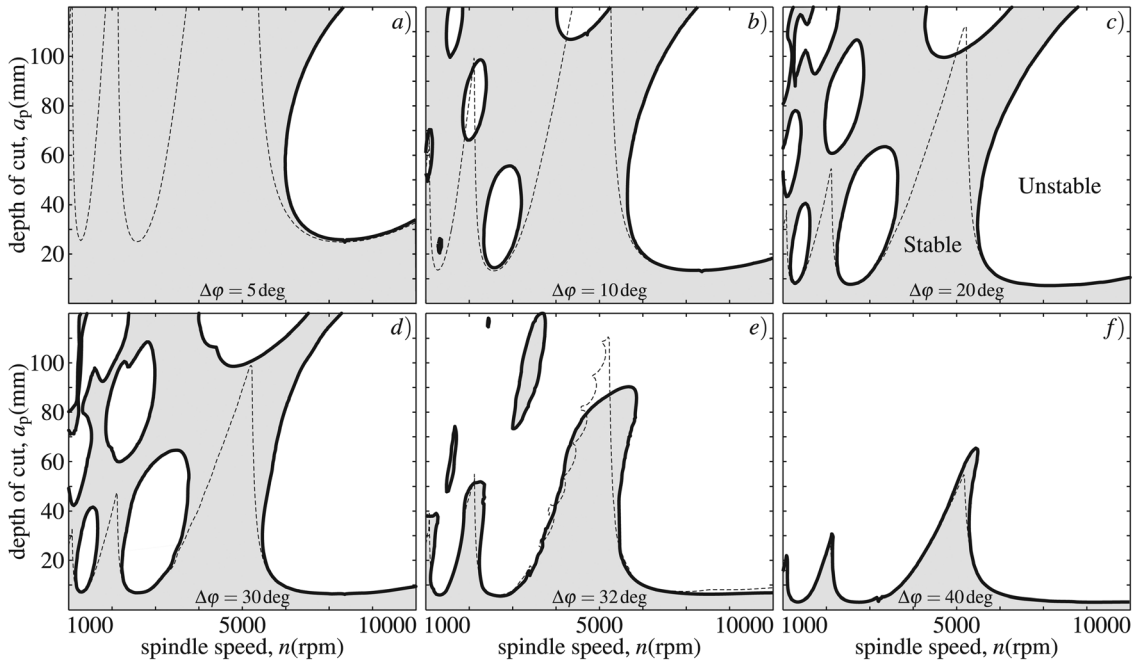

Fig. 4 Linear stability of machining process performed by milling tools with nonuniform helices with symmetric engagement defined by $\Delta\varphi$ (thick continuous line) besides the linear stability of processes performed by a conventional milling tool (thin dashed lines)

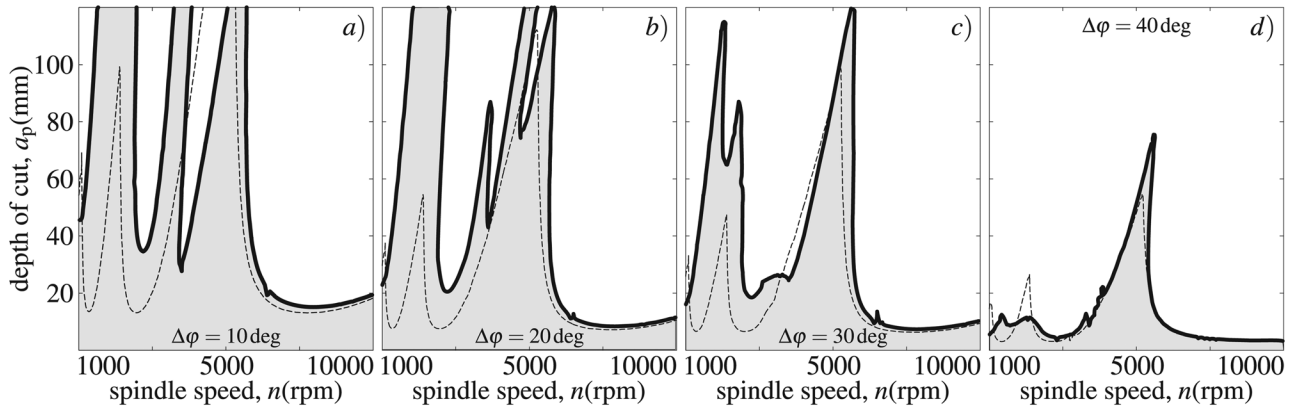

Fig. 5 Linear stability of machining process performed by harmonically varied helix milling tools with symmetric engagement defined by $\Delta\varphi$ (thick continuous line) besides the linear stability of processes performed by a conventional milling tool (thin dashed lines)

Table 1 Modal parameters used for simulations

$\omega_{n\,[1,2]}$ (Hz)	$\xi_{1,2}$ (%)	$k_{1,2}$ (N/μm)	Direction
410	2	20	(x and y)

parameters are usually measured by modal tap-testing using accelerometers and modal hammer. Two sets of numerical calculations were performed related to nonuniform helix angles with $\bar{\eta}_i = 30, 34, 30, 34$ deg and related to a tool with harmonic variation on its edges with wavelength $L_h = 15$ mm, amplitude $a_h = 10$ deg, and uniform phaseshift $\psi_{h,i}$.

Note that the presented stability charts include practically unrealistic parameter domains especially with respect to high depths of cut. However, the extended parameter domains help to identify intricate stability properties of the process. It can be observed in Fig. 4(*d*) and in Figs. 5(*a*)–5(*c*) that these tools have good dynamic properties for high axial depths of cut with extremely high material removal rate without leading to self-excited vibrations.

As it can be recognized in Fig. 4, the tool with nonuniform helix angles has a completely different dynamical behavior compared to the conventional milling tools of uniform helix angle. However, this effect decreases as the symmetric immersion angle $\Delta\varphi$ increases. In case of low symmetric engagement, the milling process performed by a nonuniform constant helix tool shows large stable domain in contrast with the conventional milling where the well-known lobe structure survives [28]. As the symmetric immersion is increased, special instability lenses show up, while the large stable domain in between becomes separated into disjunct stable islands ending up at the traditional lobe structure (Figs. 4(*b*)–4(*d*)). The unstable lenses seem to be located along steep lines starting from the origin.

A series of stability charts are also shown in Fig. 5 in case of different symmetric engagement angles $\Delta\varphi$ for milling processes with harmonically varied helix tools. It can be seen that the special stable tongues are gradually lost with the increase of the symmetric immersion angle $\Delta\varphi$ (Figs. 5(*a*)–5(*c*)). This effect was not recognized in Ref. [29] where only one vibration mode was modeled and the stable tongues remained important even for half-immersion down milling. In both cases (Figs. 4 and 5), the stability limits increase at low spindle speeds in case of low symmetric engagements. Note, however, this is essentially different from the increased linear stability caused by the process damping effect [30] at low spindle speeds, in spite of the fact that similar distributed delay models may also be used to explain the process damping phenomenon [7,31,32].

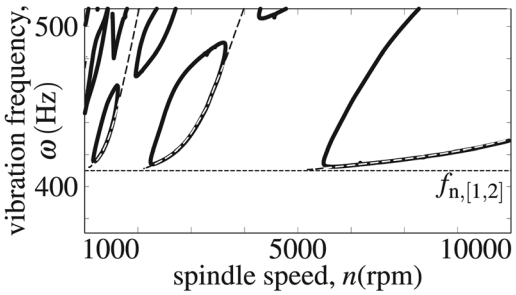

Fig. 6 The dominant (chatter) frequencies along the linear stability in the case of nonuniform constant helix tools Fig. 4(*c*) (dashed lines represents the dominant vibration frequencies of the same operation with conventional tool)

In Fig. 6, the dominant vibration frequencies [33] are plotted in case of a nonuniform helix tool for a milling process with symmetric engagement angle $\Delta\varphi = 20$ deg (Fig. 4(*c*)). It can be seen that the instability lenses that are located near to the standard linear stability limits have dominant chatter frequencies close to the natural frequencies of the system. Instability lenses at higher depths of cut regions correspond to higher dominant frequencies further away from the natural frequencies. This is against the rule of thumb that dominant chatter frequencies are in the neighborhood to the natural ones.

6 Conclusions

This work was motivated by the fact that continuous variation of the helix angle causes distribution of the regeneration between subsequent edges. A general mechanical model was presented, which is suitable to take into account the weight distribution of the regeneration occurring in the system. The shape of the weight distribution function was presented and discussed for nonuniform and harmonically varied helix angle cases.

Case studies were provided to show the relevant dynamic behavior of these cutters. Examples with two identical modes were presented, and the differences between these and the single mode models were highlighted from cutting stability viewpoint [29].

The calculations showed that special instability lenses occur in the stability chart in case of nonuniform constant helix angle milling tools. The size of these instability lenses decrease and they line up toward the low spindle-speed region. The size of the lenses shrink to a degree where the stable region above them may become practically realizable: cutting can be performed at extremely high depth of cut regions.

In case of harmonic variable helix angle milling tools, the calculations showed that large stable tongues are formed at the low spindle-speed domain, while they loose their importance as the process becomes less interrupted.

In summary, the developed distributed delay model and the examples explored some intricate stability properties of the varying helix angle tools that can be utilized both in designing new milling cutters and in identifying cutting parameter regions of extremely high material removal rates.

Acknowledgment

This research was partially supported by the Hungarian National Science Foundation under Grant No. OTKA K83890, by the EU FP7 Dynxperts (260073/FP7-2010-NMP-ICT-FoF), and the New Hungary Development Plan (Project ID: TÁMOP-4.2.1/B-09/1/KMR-2010-0002). The really rare harmonically variable milling tool was kindly provided by Prof. Gy. Matyasi, Department on Manufacturing Sciences and Technology, Budapest University of Technology and Economics.

Nomenclature

a_h = amplitude of the harmonical variation
f = feed per revolution in the x direction
g = screen function
h = chip thickness
L_h = wavelength of the harmonical variation
N = number of flutes
R = radius of the tool envelope
$\mathbf{f}$ = specific force
$\mathbf{f}(h)$ = empirical cutting force characteristics
$\mathbf{F}$ = resultant cutting force
$\mathbf{q}$ = modal coordinates
$\mathbf{u}$ = perturbation around the periodic stationary solution
$\mathbf{z}$ = discretized state of the system
$\mathbf{B}$ = discretized solution operator (step matrix)
$\mathbf{U}$ = mass normalized modal transformation matrix
$\mathbf{W}$ = weight distribution function
δ = angle variation around the mean helix angle $\bar{\eta}$
η = helix angle
θ = delayed time
ξ = damping factor
φ = position angle of the edge compared to the y axis
φ_p = pitch angle
φ_η = lag angle
Φ_p = amplitude of the pitch angle variation
ψ_h = phase shift of the harmonical variation
ω_n = natural angular frequency
$\Omega = n$ = spindle speed
Φ = transition matrix

References

[1] Tlusty, J., and Spacek, L., 1954, *Self-Excited Vibrations on Machine Tools*, Nakl. CSAV, Prague, Czech Republic.
[2] Tobias, S., 1965, *Machine-Tool Vibration*, Blackie, Glasgow.
[3] Stépán, G., 1989, *Retarded Dynamical Systems*, Longman, London.
[4] Farkas, M., 1994, *Periodic Motions*, Springer-Verlag, Berlin/New York.
[5] Hale, J., 1977, *Theory of Functional Differential Equations*, Springer-Verlag, New York.
[6] Bellen, A., and Zennaro, M., 2003, *Numerical Methods for Delay Differential Equations*, Oxford University, New York.
[7] Stépán, G., 2001, "Modelling Nonlinear Regenerative Effects in Metal Cutting," Phil. Trans. R. Soc. Lond. A, **359**, pp. 739–757.
[8] Takacs, D., Orosz, G., and Stépán, G., 2009, "Delay Effects in Shimmy Dynamics of Wheels With Stretched String-Like Tyres," Eur. J. Mech. A/Solids, **28**, pp. 516–525.
[9] Insperger, T., and Stepan, G., 2004, "Stability Analysis of Turning With Periodic Spindle Speed Modulation Via Semi-discretization," J. Vib. Control, **10**, pp. 1835–1855.
[10] Zatarain, M., Bediaga, I., Muñoa, J., and Lizarralde, R., 2008, "Stability of Milling Processes With Continuous Spindle Speed Variation: Analysis in the Frequency and Time Domains, and Experimental Correlation," CIRP Ann., **57**(1), pp. 379–384.
[11] Dombovari, Z., Altintas, Y., and Stepan, G., 2010, "The Effect of Serration on Mechanics and Stability of Milling Cutters," Int. J. Mach. Tools Manuf., **50**(6), pp. 511–520.
[12] Merdol, S. D., and Altintas, Y., 2004, "Mechanics and Dynamics of Serrated Cylindrical and Tapered End Mills," ASME J. Manuf. Sci. Eng., **126**(2), pp. 317–326.
[13] Budak, E., 2003, "An Analytical Design Method for Milling Cutters With Nonconstant Pitch to Increase Stability, Part I: Theory," ASME J. Manuf. Sci. Eng., **125**(1), pp. 29–34.
[14] Sellmeier, V., and Denkena, B., 2011, "Stable Islands in the Stability Chart of Milling Processes due to Unequal Tooth Pitch," Int. J. Mach. Tools Manuf., **51**(2), pp. 152–164.
[15] Imani, B. M., Sadeghi, M. H., and Nasrabadi, M. K., 2008, "Effects of Helix Angle Variations on Stability of Low Immersion Milling," IUST Int. J. Eng. Sci., **19**(5), pp. 115–122.
[16] Turner, S., Merdol, D., Altintas, Y., and Ridgway, K., 2007, "Modelling of the Stability of Variable Helix End Mills," Int. J. Mach. Tools Manuf., **47**(9), pp. 1410–1416.
[17] Sims, N., Mann, B., and Huyanan, S., 2008, "Analytical Prediction of Chatter Stability for Variable Pitch and Variable Helix Milling Tools," J. Sound Vib., **317**(3–5), pp. 664–686.
[18] Song, Q., Ai, X., and Zhao, J., 2011, "Design for Variable Pitch End Mills With High Milling Stability," Int. J. Adv. Manuf. Technol., **55**, pp. 891–903.
[19] Yusoff, A. R., and Sims, N. D., 2011, "Optimisation of Variable Helix Tool Geometry for Regenerative Chatter Mitigation," Int. J. Mach. Tools Manuf., **51**(2), pp. 133–141.
[20] Otto, A., and Radons, G., 2012, "Frequency Domain Stability Analysis of Milling Processes With Variable Helix Tools," 9th International Conference on High Speed Machining.
[21] Insperger, T., and Stepan, G., 2002, "Semi-Discretization Method for Delayed Systems," Int. J. Numer. Methods Eng., **55**, pp. 503–518.
[22] Altintas, Y., 2000, *Manufacturing Automation: Metal Cutting Mechanics, Machine Tool Vibrations, and CNC Design*, Cambridge University, Cambridge.
[23] Altintas, Y., Engin, S., and Budak, E., 1999, "Analytical Stability Prediction and Design of Variable Pitch Cutters," ASME J. Manuf. Sci. Eng., **121**(2), pp. 173–178.
[24] Ferry, W. B., and Altintas, Y., 2008, "Virtual Five-Axis Flank Milling of Jet Engine Impellers—Part I: Mechanics of Five-Axis Flank Milling," ASME J. Manuf. Sci. Eng., **130**(1), p. 011005.
[25] Insperger, T., and Stepan, G., 2011, *Semi-Discretization for Time-Delay Systems: Stability and Engineering Applications*, Springer, New York.
[26] Henninger, C., and Eberhard, P., 2008, "Improving the Computational Efficiency and Accuracy of the Semi-Discretization Method for Periodic Delay-Differential Equations," Eur. J. Mech. A/Solids, **27**(6), pp. 975–985.
[27] Insperger, T., 2010, "Full-Discretization and Semi-Discretization for Milling Stability Prediction: Some Comments," Int. J. Mach. Tools Manuf., **50**(7), pp. 658–662.
[28] Szalai, R., Stépán, G., and Hogan, S., 2004, "Global Dynamics of Low Immersion High-Speed Milling," Chaos, **14**(4), pp. 1069–1077.
[29] Dombovari, Z., and Stepan, G., 2011, "The Effect of Harmonic Helix Angle Variation on Milling Stability," Proceedings of DETC2011.
[30] Altintas, Y., Eynian, M., and Onozuka, H., 2008, "Identification of Dynamic Cutting Force Coefficients and Chatter Stability With Process Damping," CIRP Ann., **57**(1), pp. 371–374.
[31] Dombovari, Z., and Stepan, G., 2010, "Experimental and Theoretical Study of Distributed Delay in Machining," Proceedings of 9th IFAC Workshop on Time Delay Systems, Prague, pp. 1–5.
[32] Bachrathy, D., and Stepan, G., 2010, "Time-Periodic Velocity-Dependent Process Damping in Milling Processes," 2nd International CIRP Process Machine Interaction (PMI) Conference.
[33] Dombovari, Z., Iglesias, A., Zatarain, M., and Insperger, T., 2011, "Prediction of Multiple Dominant Chatter Frequencies in Milling Processes," Int. J. Mach. Tools Manuf., **51**(6), pp. 457–464.